Available online at www.sciencedirect.com
ScienceDirect
Journal of Sound and Vibration 308 (2007) 1–11
JOURNAL OF SOUND AND VIBRATION
www.elsevier.com/locate/jsvi

On dissipation-induced destabilization and brake squeal: A perspective using structured pseudospectra

Patrick Kessler[a], Oliver M. O'Reilly[a,*], Anne-Lise Raphael[b], Maciej Zworski[c]

[a]*Department of Mechanical Engineering, University of California at Berkeley, Berkeley, CA 94720, USA*
[b]*Département de Mathématiques Appliquées, École Polytechnique, F-91128 Palaiseau Cedex, France*
[c]*Department of Mathematics, University of California at Berkeley, Berkeley, CA 94720, USA*

Received 15 August 2005; received in revised form 2 October 2006; accepted 14 June 2007
Available online 4 September 2007

Abstract

Numerous linearizations of mechanical systems feature non-normal operators. This is particularly the case in follower force systems, gyroscopic systems and models for squealing brakes. In this paper, it is shown that a pseudospectral analysis can illuminate features of these systems including dissipation-induced destabilization and high-eigenvalue sensitivity to parameter variation.

1. Introduction

A mechanican attempting to subdue an energetic and unstable device will immediately think of using dissipation to remove excess energy. In many cases, this strategy is entirely successful, and so it is one of the most surprising results in engineering that dissipation can actually cause instability in some machines. Dissipation-induced destabilization occurs in a wide class of mechanisms including follower force and gyroscopic systems [1–3]. One of the results we will show in this paper is that it also occurs in certain models for brakes, where instability is used as an indicator of brake squeal.

Our goal in this paper is to use the pseudospectral perspective [4,5] to shed light on dissipation-induced destabilization. We put particular emphasis on a variant of the pseudospectrum known as a structured pseudospectrum [6], that ends up being useful in the analysis of mechanical systems. Generally, the pseudospectral perspective is well-suited to systems such as brake models, where high sensitivity to parameter variations can make squeal prediction and suppression difficult (see for example Refs. [7,8]). The work presented in this paper also complements existing works on eigenvalue sensitivity in follower force systems and brake models, see for example Refs. [1,7,9].

In Section 2 we provide background on pseudospectra, and in Section 3, we introduce structured pseudospectra. These concepts can arise from questions about the behavior of the linear system

$$\dot{x} = Ax, \tag{1}$$

*Corresponding author. Tel.: +1 510 642 0877; fax: +1 510 642 6123.
E-mail address: oreilly@berkeley.edu (O.M. O'Reilly).

0022-460X/$ - see front matter © 2007 Elsevier Ltd. All rights reserved.
doi:10.1016/j.jsv.2007.06.066

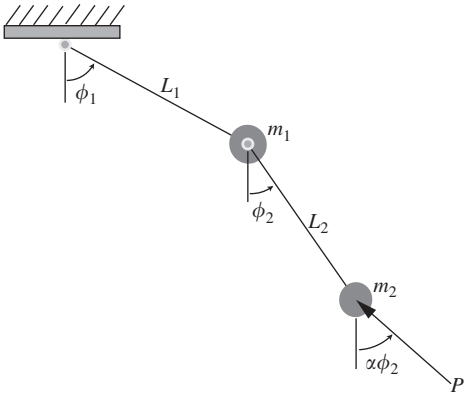

Fig. 1. Schematic of the Ziegler pendulum. The parameters and coordinates for this system are described in Section 1, as well as in Appendix A.

which are usually answered by considering the eigenvalues of A. The set of these eigenvalues is called the *spectrum* of A and is denoted Spec(A). Unfortunately there are cases for which Spec(A) does a poor job of describing the behavior of Eq. (1). These cases motivate the *ε-pseudospectrum* of A, which is denoted as $\Lambda_\varepsilon(A)$, and defined by

$$\Lambda_\varepsilon(A) = \{\lambda \in \mathrm{Spec}(A + \delta A), \text{ where } \|\delta A\| < \varepsilon\}. \tag{2}$$

In this definition, δA can be *any* perturbation to A, provided its norm[1] is less than ε. Although consideration of all possible perturbations is often useful, there are many problems in which the perturbations to A are naturally restricted. For instance when A corresponds to a mechanical system, the only possible perturbations may correspond to variations of specific parameters such as damping coefficients in follower force systems, and lining stiffness coefficients in models for brakes. In this paper, we restrict the structure of δA in Eq. (2) and we study the corresponding subset of $\Lambda_\varepsilon(A)$, known as a *structured ε-pseudospectrum*. We show that the structured ε-pseudospectrum illuminates existing results on dissipation-induced destabilization and brake squeal prediction.

In Section 4, we demonstrate the advantages of the pseudospectral perspective by analyzing the Ziegler pendulum, which consists of two masses connected by rigid links and viscoelastic hinges (see Fig. 1). The links are oriented by the angles ϕ_1 and ϕ_2, and a follower force P acting on the second mass is oriented by the angle $\alpha\phi_2$. (In the remainder of the paper we frequently refer to the nondimensionalization of P, given by $F = PL_2/k_2$.) The viscoelastic hinges are characterized by stiffness values k_1 and k_2 and damping values b_1 and b_2. A complete description of the Ziegler pendulum and its equations of motion is given in Appendix A and also in Ref. [2]. Several classical phenomena associated with this system are easy to see using a structured ε-pseudospectrum in which the perturbations δA in Eq. (2) are restricted so that they correspond to changes in the viscous damping of the pendulum joints. The linearization of the Ziegler pendulum about the trivial equilibrium state has a canonical form that encompasses a large family of mechanical systems, including brake models[2] used in the study of brake squeal. As a result, brake models and follower force systems have similar pseudospectral properties, as we discuss in Section 5.

The phenomenon of dissipation-induced destabilization in mechanical systems has a long history—for references and comments, we refer the reader to Refs. [2,11–13]. Relevant background material on brake squeal can be found in the reviews [10,14]. Material on pseudospectra can be found in Ref. [4] and in Ref. [5], and material on structured pseudospectra can be found in Refs. [15–17].

[1]In this paper *norm* will always indicate the standard 2-norm.
[2]These models date to North [10] (see, for example, Ref. [9]).

2. Background on pseudospectra

The pseudospectrum of a matrix A can be motivated by questions about the behavior of the associated differential equation $\dot{x} = Ax$. We say that the equilibrium $x = 0$ of the linear system $\dot{x} = Ax$ is asymptotically stable if all the eigenvalues λ of A satisfy $\mathrm{Re}(\lambda) < 0$. It is indeed true that

$$|x(t)| \leqslant C \exp\left(t \max_{\lambda \in \mathrm{Spec}(A)} \mathrm{Re}(\lambda) \right) \tag{3}$$

as $t \to \infty$, with an additional prefactor of t^k in some cases of multiple eigenvalues. However, if A is *nonnormal*, (that is, if $A^{\mathrm{T}}A \neq AA^{\mathrm{T}}$), then it is well-known that this asymptotic estimate can be highly *nonuniform*, especially if the dimension of A is large. Non-uniformity means that C may have to be extremely large for the inequality to hold, clearly decreasing the usefulness of the estimate. This fact encourages further consideration of nonuniformity; we note that nonuniformity is closely related to the behavior of the resolvent $R(z)$ of the matrix A.

The resolvent[3] of A is a matrix valued function defined by

$$R(z) = (zI - A)^{-1}. \tag{4}$$

If A is normal, then the norm of the resolvent is inversely proportional to the distance between $z \in \mathbb{C}$ and the spectrum of A,

$$\|R(z)\| = \mathrm{dist}(z, \mathrm{Spec}(A))^{-1}. \tag{5}$$

The situation is dramatically different however when A is nonnormal. In this case, the norm of the resolvent of A may be totally unrelated to the distance between z and the eigenvalues of A. This motivates the following definition of the ε-*pseudospectrum* of A:

$$\Lambda_\varepsilon(A) = \{\lambda \in C \text{ such that } \|R(\lambda)\| > 1/\varepsilon\}. \tag{6}$$

This definition is in fact equivalent to Eq. (2). The definition in Eq. (2) highlights the relation between $\Lambda_\varepsilon(A)$ and spectral instability.

Having defined the ε-pseudospectrum, we now present an example. In Fig. 2 we show ε-pseudospectra (with $\varepsilon = 0.001$) corresponding to the Ziegler pendulum with the dimensionless force $F = 0.2$ in image (a) and $F = 2.0$ in image (b). In both images, there are four purely imaginary eigenvalues related by reflective symmetry about the real axis, and so we only show the two that are positive. Each eigenvalue (labeled λ) is at the center of a roughly circular region (with radius labeled r). The ε-pseudospectrum in images (a) and (b) consists of the union of these circular regions. In both images, a section of the imaginary axis is removed to improve the display. As F increases, the ε-pseudopectrum grows larger, reflecting an increase in the sensitivity of the system spectrum to perturbations. Furthermore, as F increases, the operator associated with the Ziegler pendulum becomes increasingly non-normal. We recall that sensitivity to perturbations is characteristic of non-normal systems.

Many of the perturbations δA used to create Fig. 2 are not physically realistic (or realizable). To find perturbations that *are* realistic, we need to examine the structure of A. For a wide class of mechanical systems including the two considered in this paper, A has the following canonical form:

$$A = \begin{bmatrix} 0 & I \\ -M^{-1}K & -M^{-1}D \end{bmatrix}. \tag{7}$$

Here, K is a matrix with a symmetric part that corresponds to conservative forces, and with an asymmetric part that contains contributions from either the follower forces or, in the case of brake models, from friction forces. M is a symmetric positive-definite matrix called the "mass" matrix, and D is a matrix that represents linear viscous damping. In the absence of damping, Eq. (7) corresponds to a reversible dynamical system, but because $K \neq K^{\mathrm{T}}$, this system is not Hamiltonian [2]. Loosely speaking, as K becomes increasingly asymmetric,

[3]It is useful to note that the resolvent $R(s)$ is the Laplace transform of the matrix exponential e^{tA}, and can be expressed as a polynomial function of A using the Fadeev–Fadeeva formulae [18,19].

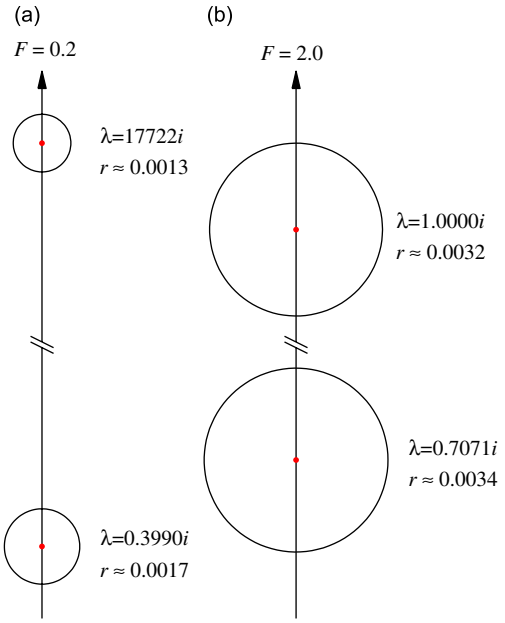

Fig. 2. These images show ε-pseudospectra of nonnormal matrices corresponding to the Ziegler pendulum for different values of F. These images were obtained with the help of EigTool [20].

the matrix A becomes increasingly nonnormal and pseudospectral effects manifest. In follower force systems, this occurs when the magnitude of the follower force increases. In many brake models, this occurs when the friction forces or coefficients of friction increase.[4]

3. Structured pseudospectra

Motivated by Eq. (2), we define a structured ε-pseudospectrum of the linear operator A to be

$$\Sigma_\varepsilon(A) = \{\lambda \in \mathrm{Spec}(A + \delta A) \text{ such that } \|\delta A\| < \varepsilon \text{ and } \delta A \in S\}, \tag{8}$$

where S is the set of matrices that satisfy some structural condition. To study the effects of damping and other parameter variations on the mechanical systems of interest, we will examine $\Sigma_\varepsilon(A)$ where

$$A = \begin{bmatrix} 0 & I \\ -M^{-1}K & 0 \end{bmatrix}, \tag{9}$$

and where $\delta A \in S$ in Eq. (8) indicates that δA has the following structure:

$$\delta A = \begin{bmatrix} 0 & 0 \\ -M^{-1}H & -M^{-1}D \end{bmatrix}, \tag{10}$$

with M and D positive definite. Here H represents variations in the applied forces and stiffnesses. We note that Eq. (9) is non-normal when $K \neq K^{\mathrm{T}}$.

4. Example of a follower force system

The Ziegler pendulum shown in Fig. 1 is a follower force system that experiences dissipation-induced destabilization. This phenomenon is illustrated in Fig. 3 where the pendulum position as a function of time is

[4]See Section 8 of Ref. [14] where lumped parameter models for disk brakes are discussed. A detailed discussion of the case of a large degree-of-freedom finite-element model can be found in the Appendix of Ref. [9].

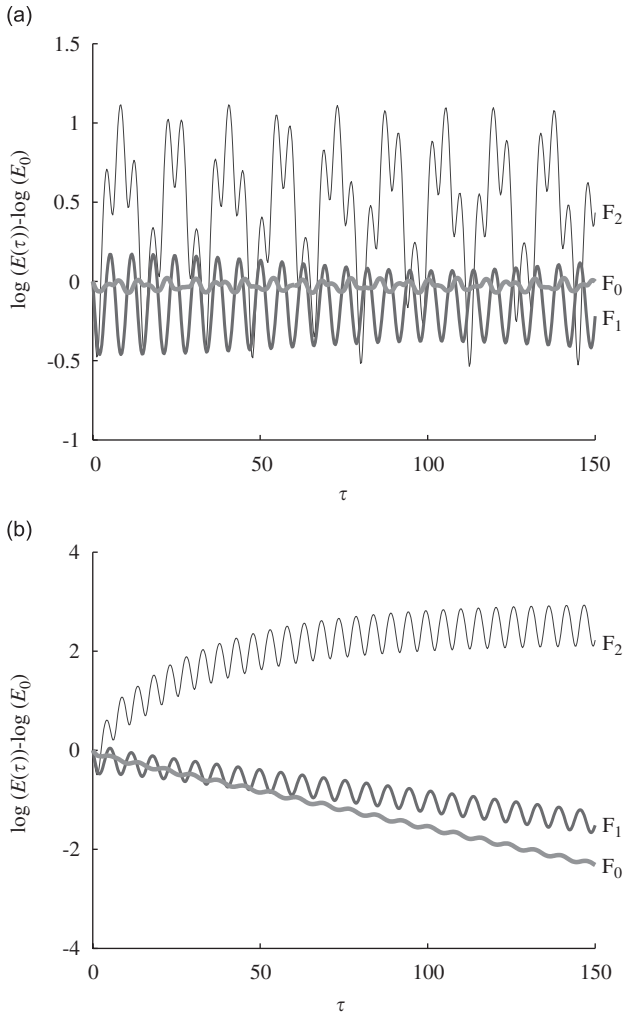

Fig. 3. Simulations showing dissipation-induced destabilization in the Ziegler pendulum. In (a) and (b) $F_0 = 0.2$, $F_1 = 1.2$, and $F_2 = 2.0$. In (a), damping is absent and the F_2 simulation is stable, while in (b) damping is present and the F_2 simulation is unstable.

determined by numerically integrating the nonlinear equations given in Appendix A. In images (a) and (b) in this figure, F takes on the values 0.2, 1.2, and 2.0, and the logarithm of the normalized total energy E is plotted as a function of a dimensionless time τ. In image (a), damping is absent, whereas in image (b), the elements of the damping matrix Eq. (11) are $c_1 = c_2 = 0.1$. (These non-dimensional coefficients are defined in Appendix A.) We see that for the smaller value of F, the equilibrium is stable both in the absence and presence of damping. For the larger value of F, the equilibrium is stable in the absence of damping, but can become unstable when damping is added.

It turns out that dissipation-induced destabilization also occurs in the linearized equations of motion for the Ziegler pendulum, given by $M\ddot{z} + D\dot{z} + Kz = 0$ where

$$M = \begin{bmatrix} m+2 & 1 \\ 1 & 1 \end{bmatrix}, \quad D = \begin{bmatrix} c_1 + c_2 & -c_2 \\ -c_2 & c_2 \end{bmatrix}, \quad K = \begin{bmatrix} 1 + \kappa - F & F - 1 \\ -1 & 1 \end{bmatrix}. \tag{11}$$

The nondimensional mass, damping, stiffness, and follower force terms m, c_i, κ, and F that we use here are defined in Appendix A. The linearized Ziegler equations can be written as $\dot{x} = Ax$ where A is the matrix in Eq. (7), with M, D, and K as given above. When D and F are zero, A has a pair of purely imaginary eigenvalues. As F increases, these eigenvalues move towards each other along the imaginary axis, merging in a

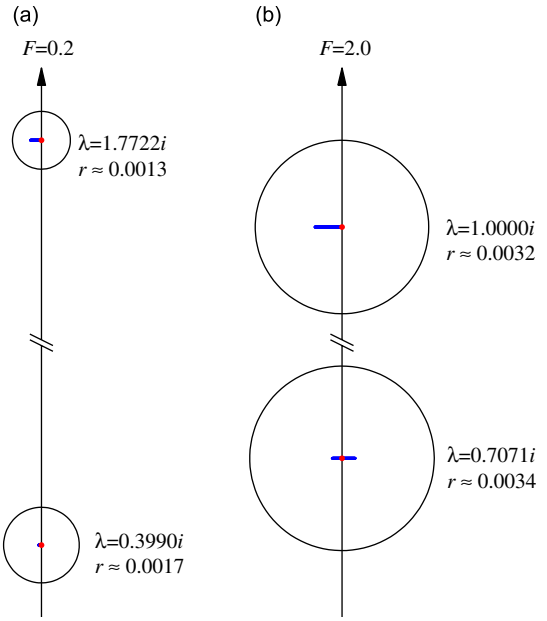

Fig. 4. Here we superpose the structured ε-pseudospectrum $\Sigma_\varepsilon(A)$ on the regular ε-pseudospectrum from Fig. 2.

reversible Hopf bifurcation[5] when F is approximately 2.086. In the presence of damping however, the eigenvalues of A can move into the right half-plane for F as low as 1.2. This is the dissipation-induced destabilization that interests us.

When $D = 0$, the operator A associated with the Ziegler pendulum is given by Eq. (9). The ε-pseudospectrum of this A does not reveal anything about dissipation-induced destabilization (see Fig. 2), although it does show that larger values of F (which cause A to be increasingly non-normal) make A more sensitive to perturbations. We illuminate the system response to dissipation by constructing a structured ε-pseudospectrum $\Sigma_\varepsilon(A)$ for the system with A and δA as given in Eqs. (9) and (10), respectively, with H in Eq. (10) set equal to 0. We generate each δA by constructing a random positive definite D with unit magnitude, and by then setting

$$\delta A = \begin{bmatrix} 0 & 0 \\ 0 & \beta M^{-1} D \end{bmatrix}, \tag{12}$$

with $\beta = \tilde{\varepsilon}/\|M^{-1}D\|$ for some $\tilde{\varepsilon} \in [0, \varepsilon)$. The random positive definite D is given by

$$D = \begin{bmatrix} \cos\theta & \sin\theta \\ -\sin\theta & \cos\theta \end{bmatrix} \begin{bmatrix} 1 & 0 \\ 0 & d_1 \end{bmatrix} \begin{bmatrix} \cos\theta & -\sin\theta \\ \sin\theta & \cos\theta \end{bmatrix}, \tag{13}$$

where θ and d_1 are random numbers on $[0, 2\pi]$ and $[0, 1]$, respectively.

In Fig. 4 we superpose a structured ε-pseudospectrum $\Sigma_\varepsilon(A)$ on an exact copy of the ε-pseudospectrum $\Lambda_\varepsilon(A)$ from Fig. 2. Our $\Sigma_\varepsilon(A)$ is generated by restricting the perturbations δA to the form Eq. (10). This restriction causes the ε-pseudospectra from Fig. 2 to collapse down to the much smaller horizontally oriented regions at the circle centers. When these smaller regions have a part in the right half-plane, (such as when $F = 2.0$), it is possible for the Ziegler pendulum to experience dissipation-induced destabilization. We examine these smaller regions in greater detail in Figs. 5 and 6.

In Fig. 5, we show structured ε-pseudospectra (with $\varepsilon = 0.001$) for the Ziegler pendulum as F increases through the values 0.2, 1.2, 1.4, 1.6, and 1.7. The structured ε-pseudospectra are the regions outlined in small dots, the system eigenvalues are the larger dots, and the vertical line in each image is the $i\mathbb{R}$ axis. As F increases, the eigenvalues move towards each other along the $i\mathbb{R}$ axis, and for some F between 0.2 and 1.2, the

[5]This event is also known as a binary flutter instability.

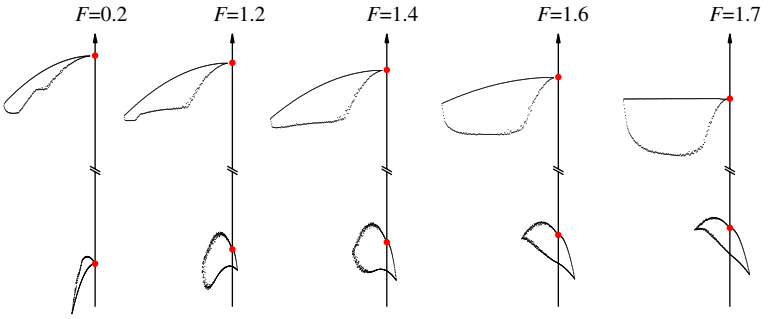

Fig. 5. These images show a progression of structured ε-pseudospectra for the Ziegler pendulum.

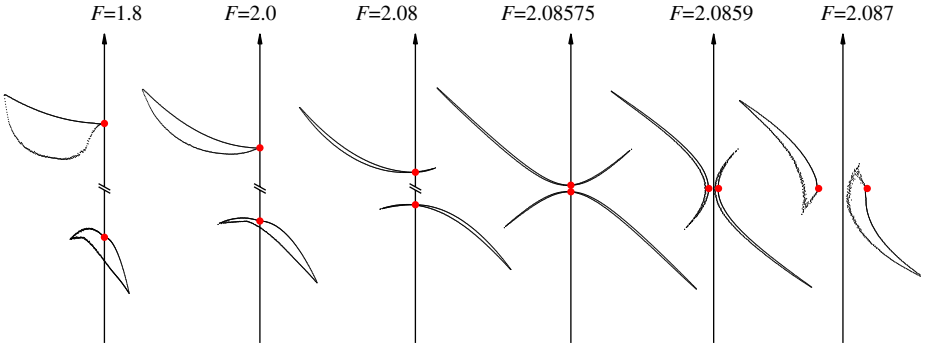

Fig. 6. These images continue the progression from Fig. 5.

structured ε-pseudospectrum moves into the right half-plane. The regions surrounding each eigenvalue are scaled and translated, and data below the real axis is omitted. Actual parameters for these regions are given in Appendix B. It is evident from the first image in Fig. 5 that for small F, dissipation stabilizes the equilibrium. However, as F gets larger, the non-normality of A increases and dissipation can induce instability. As is evident from the results for $F \geqslant 2.08$, the destabilization can occur in either pair of eigenvalues.

In Fig. 6, we continue the progression from Fig. 2, with F values of 1.8, 2, 2.08, 2.08575, 2.0859, and 2.087. In 1952, Ziegler [3] showed that the merging of the eigenvalues suggested by the transition from the fourth image to the fifth image above occurs at the exact value $F = \frac{7}{2} - \sqrt{2}$.

5. Brake squeal

We now consider the usefulness of structured ε-pseudospectra in predicting brake squeal. As may be surmised from the vast literature on this topic, brake squeal is an elusive phenomenon for which complete suppression is difficult. Here we consider a simple brake model (see Fig. 7) with a linearization A that becomes increasingly non-normal as the onset of squeal is approached. As a consequence of this non-normality, the spectrum of A becomes more sensitive to perturbations, and small changes to the system parameters greatly affect the onset of squeal. Our comments here are in accord with the independent observations on this sensitivity that have appeared in Refs. [7,8]. If we add *large* amounts of dissipation to the system, then the eigenvalues develop negative real parts, and the pseudospectral effects are reduced. This is in agreement with the common practice of using dissipation as a squeal suppression mechanism.[6] Small amounts of damping however may give rise to instability.

Our brake model is a discrete two degree-of-freedom system first described by North in Ref. [10], (see Fig. 7). In this model, the brake rotor is represented by a tilted rigid rod of mass m, moment of inertia I, length

[6]For additional background on squeal suppression mechanisms, see Ref. [14].

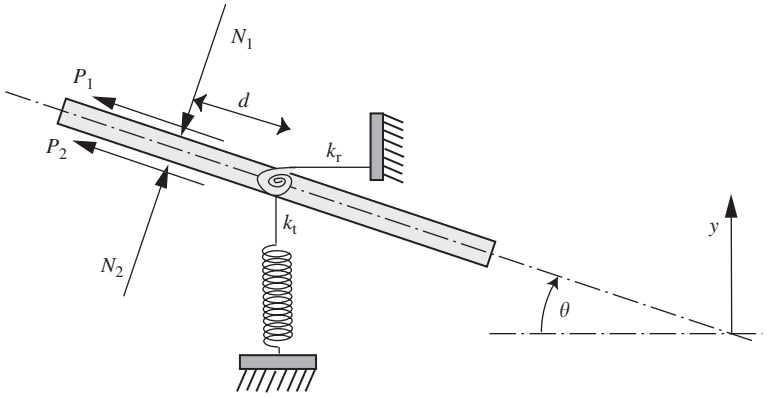

Fig. 7. Schematic of North's two degree-of-freedom model for a disk brake, (adapted from Ref. [10] with some changes in notation).

L and thickness $2h$. The brake pads in contact with the rotor are incorporated into the model by the normal forces N_1 and N_2, and by the frictional forces P_1 and P_2. The translational and rotational degrees of freedom of the rod are denoted by y and θ, respectively. To model the stiffness of the rotor, we subject the rod to a torsional spring of stiffness k_r and a linear spring of stiffness k_t. The flexibility of the brake pads is included in the model by a linear spring of stiffness $k_p/2$ for each pad. The normal forces are assumed to be

$$N_1 = \frac{k_p}{2}(y + \mathrm{d}\theta) + N_0, \quad N_2 = -\frac{k_p}{2}(y + \mathrm{d}\theta) + N_0, \tag{14}$$

where N_0 accounts for a static preload between the brake pads and the rotor, and where d is the dimension shown in Fig. 7. The corresponding expressions for the frictional forces are:

$$P_1 = \mu N_1, \quad P_2 = \mu N_2, \tag{15}$$

where μ is a coefficient of friction. The (dimensionless) linearized equations of motion for this model are given by $M\ddot{z} + D\dot{z} + Kz = 0$ where

$$z = \begin{bmatrix} \dfrac{y}{d} \\ \theta \end{bmatrix}, \quad M = \begin{bmatrix} 1 & 0 \\ 0 & \dfrac{1}{md^2} \end{bmatrix},$$
$$K = \begin{bmatrix} 1 + \kappa_p & -\eta + \kappa_p \\ (1+\sigma)\kappa_p & (1+\sigma)\kappa_p + \kappa_r \end{bmatrix} \tag{16}$$

and where D is a positive definite matrix representing the effects of damping. The dimensionless parameters in these matrices are:

$$\kappa_p = \frac{k_p}{k_t}, \quad \kappa_r = \frac{k_r}{d^2 k_t}, \quad \sigma = \frac{\mu h}{d}, \quad \eta = \frac{2\mu N_0}{k_t d}, \tag{17}$$

where the frequency $\sqrt{k_t/m}$ is used to non-dimensionalize time. The system equations of motion can be written as $\dot{x} = Ax$ where A is given by the canonical form Eq. (7), just as it was for the Ziegler pendulum. Recall that A is nonnormal when $K \neq K^{\mathrm{T}}$, which in our system occurs when

$$\mu + \sigma\kappa_p \neq 0 \iff \mu\left(\frac{k_p}{k_t}\frac{h}{d} + 1\right) \neq 0. \tag{18}$$

This condition always holds because the friction coefficient μ is never zero. The structured ε-pseudospectra for this system are qualitatively similar to those of the Ziegler pendulum, with the friction coefficient μ in the brake model analogous to the follower force F in the Ziegler pendulum. The introduction of *small* amounts of damping can cause the system eigenvalues to move into the right half plane, for lesser friction coefficient values than those needed to reach the reversible Hopf bifurcation in the case when no damping is present.

6. Concluding remarks

We have used structured pseudospectra to illustrate the presence of dissipation-induced destabilization in follower force systems and brake models. Related results also apply for gyroscopic systems, but are so similar that we do not present them here.[7] We point out that non-normal matrices which have a more general structure than Eq. (7) can be found in the literature (see, e.g., Ref. [8]), and that a structured pseudospectral analysis can also be performed for them.

Acknowledgments

This research was partially supported by grants from the Center for Pure and Applied Mathematics at the University of California at Berkeley. The work of Maciej Zworski was partially supported by grant number DMS-0200732 from the National Science Foundation.

Appendix A. Equations of motion for the Ziegler pendulum

The pendulum system shown in Fig. 1 consists of a mass m_1 attached by a link L_1 to a fixed base, and a mass m_2 attached by a link L_2 to the mass m_1. The links L_1 and L_2 make angles ϕ_1 and ϕ_2, respectively with a fixed line of reference. The points of attachment are viscoelastic hinges, endowed with torsional stiffness and damping. We quantify the torsional stiffness at the first and second hinges by the coefficients k_1 and k_2, respectively. These coefficients have units of [force] × [distance]. The damping coefficients associated with the first and second hinges are denoted b_1 and b_2, respectively, and have units of [force] × [distance] × [time]. A follower force of magnitude F acts on m_2 at an angle $\alpha\phi_2$ with respect to the line of reference from before. For good measure we include gravity g acting on both masses in the direction of the line of reference.

We first use the frequency $\nu = \sqrt{k_2/L_2^2 m_2}$ to establish the following non-dimensional values:

$$F = \frac{PL_2}{k_2}, \quad \kappa = \frac{k_1}{k_2}, \quad l = \frac{L_1}{L_2}, \quad m = \frac{m_1}{m_2} - 1,$$
$$\gamma = \frac{g}{\nu^2}, \quad c_1 = \frac{b_1 \nu}{k_2}, \quad c_2 = \frac{b_2 \nu}{k_2}, \quad \tau = t\nu. \tag{A.1}$$

With the understanding that a superposed dot indicates differentiation with respect to τ, the Ziegler pendulum equations of motion are given by

$$\begin{bmatrix} l^2(m+2) & l\cos(\phi_1-\phi_2) \\ l\cos(\phi_1-\phi_2) & 1 \end{bmatrix} \begin{bmatrix} \ddot{\phi}_1 \\ \ddot{\phi}_2 \end{bmatrix}$$
$$= l\sin(\phi_1-\phi_2) \begin{bmatrix} -\dot{\phi}_2^2 \\ \dot{\phi}_1^2 \end{bmatrix} + \begin{bmatrix} -(\kappa+1) & 1 \\ 1 & -1 \end{bmatrix} \begin{bmatrix} \phi_1 \\ \phi_2 \end{bmatrix} + F \begin{bmatrix} \sin(\phi_1 - \alpha\phi_2) \\ l^{-1}\sin((1-\alpha)\phi_2) \end{bmatrix}$$
$$+ \begin{bmatrix} -(c_1+c_2) & c_2 \\ c_2 & -c_2 \end{bmatrix} \begin{bmatrix} \dot{\phi}_1 \\ \dot{\phi}_2 \end{bmatrix} - \gamma \begin{bmatrix} l(m+2)\sin\phi_1 \\ \sin\phi_2 \end{bmatrix}. \tag{A.2}$$

[7] A good system to explore these results is Example 4.6.1 in Ref. [13].

The non-dimensional kinetic, spring potential, and gravitational potential energies of the system are:

$$\begin{aligned}
\mathrm{KE} &= \tfrac{1}{2}l^2(m+2)\dot{\phi}_1^2 + \tfrac{1}{2}\dot{\phi}_2^2 + l\dot{\phi}_1\dot{\phi}_2\cos(\phi_1-\phi_2),\\
\mathrm{PE}_s &= \tfrac{1}{2}(\kappa\phi_1^2 + (\phi_2-\phi_1)^2),\\
\mathrm{PE}_g &= -\gamma(m+2)l\cos\phi_1 - \gamma\cos\phi_2.
\end{aligned} \tag{A.3}$$

With $\alpha = 1$ and $\gamma = 0$, the system linearization about zero is given by

$$M\begin{bmatrix}\ddot{\phi}_1\\ \ddot{\phi}_2\end{bmatrix} + D\begin{bmatrix}\dot{\phi}_1\\ \dot{\phi}_2\end{bmatrix} + K\begin{bmatrix}\phi_1\\ \phi_2\end{bmatrix} = 0, \tag{A.4}$$

where

$$M = \begin{bmatrix}m+2 & 1\\ 1 & 1\end{bmatrix}, \quad D = \begin{bmatrix}c_1+c_2 & -c_2\\ -c_2 & c_2\end{bmatrix}, \quad K = \begin{bmatrix}1+\kappa-F & F-1\\ -1 & 1\end{bmatrix}. \tag{A.5}$$

Appendix B. Data from Figs. 5 and 6

Table B1 gives the eigenvalues and structured ε-pseudospectra dimensions from Figs. 5 and 6. For each value of F, the structured ε-pseudospectrum consists of four distinct regions in $\mathbb{C}$, each containing one of the system eigenvalues. We identify each such region R by the eigenvalue it contains. The structured pseudospectrum is symmetric with respect to the real axis, and so we only give data above the real axis.

Table B1
Eigenvalues and structured ε-pseudospectra dimensions from Figs. 5 and 6

F	$\mathrm{Re}(\lambda)$	$\mathrm{Im}(\lambda)$	$\min(\mathrm{Re}(R))$	$\Delta\,\mathrm{Re}(R)$	$\min(\mathrm{Im}(R))$	$\Delta\,\mathrm{Im}(R)$
0.20000	−9.496656e − 18	1.772232e + 00	−4.918268e − 04	4.626542e − 04	1.772232e + 00	8.034621e − 08
0.20000	−1.135801e − 16	3.989923e − 01	−1.253187e − 04	1.249762e − 04	3.989923e − 01	2.221254e − 08
1.20000	−1.949384e − 17	1.434196e + 00	−5.276500e − 04	5.026811e − 04	1.434196e + 00	8.058873e − 08
1.20000	−1.949384e − 17	4.930336e − 01	−1.474492e − 04	1.723291e − 04	4.930336e − 01	2.181407e − 08
1.40000	−6.884011e − 17	1.351373e + 00	−5.503930e − 04	5.273948e − 04	1.351373e − 00	7.829293e − 08
1.40000	−4.108453e − 17	5.232507e − 01	−1.619412e − 04	2.070492e − 04	5.232507e − 01	2.859811e − 08
1.60000	−3.928148e − 17	1.258741e + 00	−5.887940e − 04	5.645737e − 04	1.258741e − 00	8.145434e − 08
1.60000	−1.152590e − 17	5.617572e − 01	−1.866597e − 04	2.697304e − 04	5.617571e − 01	6.534549e − 08
1.70000	−2.679640e − 18	1.206970e + 00	−6.204038e − 04	6.006905e − 04	1.206970e − 00	8.897478e − 08
1.70000	−2.679640e − 18	5.858529e − 01	−2.059099e − 04	3.210697e − 04	5.858528e − 01	1.069690e − 07
1.80000	−2.123300e − 17	1.149652e + 00	−6.706411e − 04	6.505671e − 04	1.149652e − 00	1.785604e − 07
1.80000	−6.522575e − 18	6.150617e − 01	−2.295368e − 04	3.949867e − 04	6.150616e − 01	1.945922e − 07
2.00000	−1.804112e − 16	1.000000e − 00	−9.831250e − 04	9.758750e − 04	9.999998e − 01	1.562333e − 06
2.00000	−4.483593e − 17	7.071068e − 01	−3.500000e − 04	8.281930e − 04	7.071053e − 01	1.572187e − 06
2.08000	−6.278791e − 16	8.797905e − 01	−3.032270e − 03	3.559450e − 03	8.797900e − 01	9.897194e − 05
2.08000	−5.723679e − 16	8.037218e − 01	−9.253781e − 04	3.424958e − 03	8.036232e − 01	9.897771e − 05
2.08575	−3.955170e − 15	8.439200e − 01	−1.032975e − 02	1.502420e − 02	8.439149e − 01	7.460492e − 03
2.08575	−4.024558e − 15	8.378837e − 01	−5.140275e − 03	1.484115e − 02	8.304282e − 01	7.460505e − 03
2.08590	−5.328282e − 03	8.408795e − 01	−5.097472e − 03	5.618368e − 03	8.312490e − 01	1.347916e − 02
2.08590	−5.328282e − 03	8.408795e − 01	−1.120838e − 02	5.860394e − 03	8.368811e − 01	1.352532e − 02
2.08700	−1.741811e − 02	8.407160e − 01	−1.717581e − 02	9.079214e − 04	8.350055e − 01	7.293936e − 03
2.08700	−1.741811e − 02	8.407160e − 01	−1.857042e − 02	1.133566e − 03	8.390573e − 01	7.310464e − 03

$\Delta\,\mathrm{Re}(R)$ denotes $\max(\mathrm{Re}(R))$–$\min(\mathrm{Re}(R))$, and $\Delta\,\mathrm{Im}(R)$ denotes $\max(\mathrm{Im}(R))$–$\min(\mathrm{Im}(R))$.

References

[1] O.N. Kirillov, A.O. Seyranian, The effect of small internal and external damping on the stability of distributed non-conservative systems, *Journal of Applied Mathematics and Mechanics* 69 (2005) 529–552.

[2] O.M. O'Reilly, N.K. Malhotra, N.S. Namachchivaya, Some aspects of destabilization of the equilibria of reversible dynamical systems with application to follower forces, *Nonlinear Dynamics* 10 (1996) 63–87.

[3] H. Ziegler, Stability criteria in elastomechanics, *Ingenieur Archiv* 20 (1) (1952) 49–56 (in German).

[4] L.N. Trefethen, M. Embree, *Spectra and Pseudospectra: The Behavior of Non-Normal Matrices and Operators*, Princeton University Press, 2005.

[5] L.N. Trefethen, Pseudospectra of linear operators, *SIAM Review* 39 (1997) 383–400.

[6] D. Hinrichsen, A.J. Pritchard, *Mathematical Systems Theory 1: Modelling, State Space Analysis, Stability and Robustness*, Springer, Berlin, 2005, pp. 530–532.

[7] J. Huang, C.M. Krousgrill, A.K. Bajaj, Modeling of automotive drum brakes for squeal and parameter sensitivity analysis, *Journal of Sound and Vibration* 289 (2006) 245–263.

[8] U. Von Wagner, D. Hochlenert, P. Hagedorn, Minimal models for the explanation of disk brake squeal, *Journal of Sound and Vibration* 302 (3) (2007) 527–539.

[9] Y.S. Lee, P.C. Brooks, D.C. Barton, D.A. Crolla, A predictive tool to evaluate disc brake squeal propensity. Part 2: system linearization and modal analysis, *International Journal of Vehicle Design* 31 (3) (2003) 309–329.

[10] M.R. North, Disc brake squeal, in: *Braking of Road Vehicles*, Automobile Division of the Institution of Mechanical Engineers, Mechanical Engineering Publications Limited, London, England, 1976, pp. 169–176.

[11] A. Bloch, P.S. Krishnaprasad, J.E. Marsden, T. Ratiu, Dissipation induced instabilities, *Annales De L'Institut H. Poincaré: Analyse Non Linéaire* 11 (1994) 37–90.

[12] G. Haller, Gyroscopic stability and its loss in systems with two essential coordinates, *International Journal of Nonlinear Mechanics* 27 (1) (1992) 113–127.

[13] D.J. Inman, *Vibration with Control, Measurement and Stability*, Prentice-Hall, Englewood Cliffs, NJ, 1989.

[14] N.M. Kinkaid, O.M. O'Reilly, P. Papadopoulos, Automotive disk brake squeal, *Journal of Sound and Vibration* 267 (1) (2003) 105–166.

[15] J. Kozánek, Resolvent of matrix polynomials, pseudospectra and inversion problems, *Selçuk Journal of Applied Mathematics* 3 (1) (2002).

[16] F. Tisseur, N.J. Higham, Structured pseudospectra for polynomial eigenvalue problems with applications, *SIAM Journal on Matrix Analysis and Applications* 23 (1) (2001) 187–208.

[17] T. Wagenknecht, J. Agarwal, Structured pseudospectra in structural engineering, Preprint: University of Bristol ⟨http://seis.bris.ac.uk/∼enxtw/⟩ *International Journal for Numerical Methods in Engineering* 64 (13) (2005) 1735–1751.

[18] S.-H. Hou, A simple proof of the Leverrier–Faddeev characteristic polynomial algorithm, *SIAM Review* 40 (3) (1998) 706–709.

[19] L.A. Zadeh, C.A. Desoer, *Linear Systems Theory: The State Space Approach*, McGraw-Hill, New York, 1963.

[20] T.G. Wright, EigTool: A graphical tool for nonsymmetric eigenproblems, Oxford University, ⟨http://www.comlab.ox.ac.uk/pseudospectra/eigtool/⟩.